Detection Spectrum Optimization of Stealth Aircraft Targets From a Space-based Infrared Platform

Xinyue Ni
Shanghai Institute of Technical Physics
Shutian Yu
Shanghai Institute of Technical Physics
Xiaofeng Su
Shanghai Institute of Technical Physics
Fansheng Chen (cfs@mail.sitp.ac.cn)
Shanghai Institute of Technical Physics https://orcid.org/0000-0003-2244-8327

Research Article

Keywords: Spectrum dynamic-modification, Signal-to-noise ratio, Optimal detection spectrum, Central wavelength

Posted Date: March 25th, 2021

DOI: https://doi.org/10.21203/rs.3.rs-315617/v1

Version of Record: A version of this preprint was published at Optical and Quantum Electronics on February 9th, 2022. See the published version at https://doi.org/10.1007/s11082-021-03451-4.

Detection spectrum optimization of stealth aircraft targets from a space-based infrared platform

Xinyue Ni[1, 3], Shutian Yu[1, 3], Xiaofeng Su[*, 1], AND Fansheng Chen[*, 1, 2, 3]

[1] *Key Laboratory of Intelligent Infrared Perception, Shanghai Institute of Technical Physics, Chinese Academy of Sciences, Shanghai, China, 200083*

[2] *Hangzhou Institute for Advanced Study, University of Chinese Academy of Sciences, Hangzhou, China, 310024*

[3] *University of Chinese Academy of Sciences, Beijing, China, 100049*

*(*author for correspondence, E-mail: fishsu@mail.sitp.ac.cn;)*

Abstract. Advances in infrared detection techniques require novel spectrum dynamic-modification strategies capable of sensing unprecedentedly low target radiant intensities. A conventional fixed-spectrum detection system cannot satisfy the effective detection of stealth aircraft targets due to complex Earth background clutter and atmospheric attenuation. Therefore, a detection method that can highlight aircraft targets is urgently needed to enhance stealth aircraft detectability. In this research, a spectrum set consisting of different bandwidths associated with a central wavelength is established. Furthermore, a signal-to-noise ratio of the stealth aircraft is computed using the established spectrum set. Finally, the optimal spectrum is selected according to the maximal signal-to-noise ratio from the spectrum set. Our numerical experiments and simulations further demonstrate that the proposed methodology can substantially strengthen the detection performance of stealth aircraft compared with traditional fixed-spectrum detection systems. This work on detection spectrum optimization paves the way to stealth aircraft detection and opens new vistas in the field of target detection technology.

Key words: Spectrum dynamic-modification; Signal-to-noise ratio; Optimal detection spectrum; Central wavelength;

1. Introduction

Detecting stealth aircraft based on a space-based infrared imaging system is currently a significant research area. Earth background clutter, atmospheric attenuation and low-infrared signature design of the aircrafts (Zheng, Q. et al. 2019; Zhang, T. et al. 2020) restrain aircraft detectability given the complex Earth IR background environment. At the aircraft's low flying altitude its infrared signatures are immersed in the background noise. Therefore, it is of considerable significance to propose a novel methodology to highlight aircraft signals in a complex IR background.

The infrared signature research of the target is the premise of analyzing its detectability (Li, N. et al. 2016; Zhou, Y. et al. 2017; Zhou, Y. et al. 2017; Chen, H. et al. 2019; Cheng, W. et al. 2019; Sun, W. et al. 2019; Wu, S. et al. 2019; Nam, J. et al. 2020). The high-temperature plume and the high-temperature of the aircraft skin produced by the stealth aircraft in high-speed flight have prominent infrared radiation characteristics. Many institutions have published extensive research focusing on infrared signatures of stealth aircraft and many have

also developed signature computational codes, which have been validated on extensive experimental data recording of aircraft (Mahulikar, S. P. et al. 2001; Johansson, M. et al. 2006; Mahulikar, S. P. et al. 2007; Veiga, IV.. 2011; Baranwal, N. et al. 2015; Sircilli, F. et al. 2015; Lee, J. H. et al. 2019; Hu, Hai.et al. 2020). However, the study on the radiation signature difference of stealth aircraft over various spectrum ranges is minimal. Many studies have focused on several specific broad-spectrums, such as 1.8~2.4μm, 2.5~3.57μm, 4~4.76μm, etc., covering two aircraft plume peak spectra along with the skin reflection radiation spectra that has high atmospheric transmittance (Willers, C. J. et al. 2014; Pan, X. et al. 2015; Mahulikar, S. P. et al. 2015; Wang, Y. et al. 2016; Gu, B. et al. 2017; Kou, T. et al. 2018; Kou, T. et al. 2018). The results show that the above spectra can make significant contributions to aircraft detection. Rao, G. A. pointed out that the narrow-spectrum detection method has better detection performance, and demonstrated the optimal detection spectrum of aircraft is 4.14~4.18μm and 4.56~4.65μm according to the plume spectral emissivity and atmospheric absorption character (Rao, G. A. et al. 2013). Yuan, H. proposed that the optimum detection spectra of a space-based system to stealth aircraft are 2.65~2.90μm and 4.25~4.50μm under the altostratus cloud background clutter (Yuan, H. et al. 2019). To the best of our knowledge, current research only analyzed specific conditions but has not comprehensively studied the factors affecting the system detection performance, including aircraft speed, flying altitude, atmospheric spectral absorption characteristics, and dynamic changes of the Earth background. The fixed-spectrum detection method cannot meet the continuous and effective detection of aircraft targets in complex dynamic scenes.

In this work, A dynamic-spectrum detection method is proposed to enhance the aircraft target detection capability based on the above problems. The infrared radiation signature of stealth aircraft and the Earth background is analyzed. The mathematical detection model of the space-based infrared system to aircraft targets in the Earth background is described. Our numerical experiments and simulations verify that the proposed method improves the aircraft detection performance significantly. The research results provide data support for the robust detection of stealth aircraft against the complex IR Earth background and a theoretical basis for the design parameters of a dynamic-spectrum detection system.

2. Mathematical model of Spectrum optimization

2.1 The aircraft radiation signature

In general, the total infrared radiation signature from the aircraft can be attributed to skin infrared radiation and plume infrared radiation, both of which meet Planck's radiation law.

In addition to thermal radiation, the aircraft skin also reflects solar radiation, which is mainly diffuse reflection due to the aircraft's special surface which is designed to not be detectable against the Earth background. Therefore, the spectral infrared radiant intensity of the aircraft skin can be expressed as

$$I_{skin}(\lambda)=\frac{\varepsilon_{skin}}{\pi}M\left(T_{skin\_ave},\lambda\right)A_{skin}+\frac{r_{diff}}{\pi}S_{sun}(\lambda,\theta)\tau_{sun}(\lambda)A_{ref} \tag{1}$$

where $\varepsilon_{skin}/r_{diff}$ are the spectral infrared emissivity and reflectivity of the skin, T_{skin_ave} is the average skin temperature, $M\left(T_{skin\_ave},\lambda\right)$ is spectral radiant emittance, A_{skin} is the projected area of the skin to the detector array, $S_{sun}(\lambda,\theta)$ is the spectral solar irradiance to the aircraft, $\tau_{sun}(\lambda)$ is the spectral atmospheric transmittance of the sun to the aircraft, A_{ref} is the effective area of the aircraft skin reflecting solar radiation, and λ is the spectral wavelength.

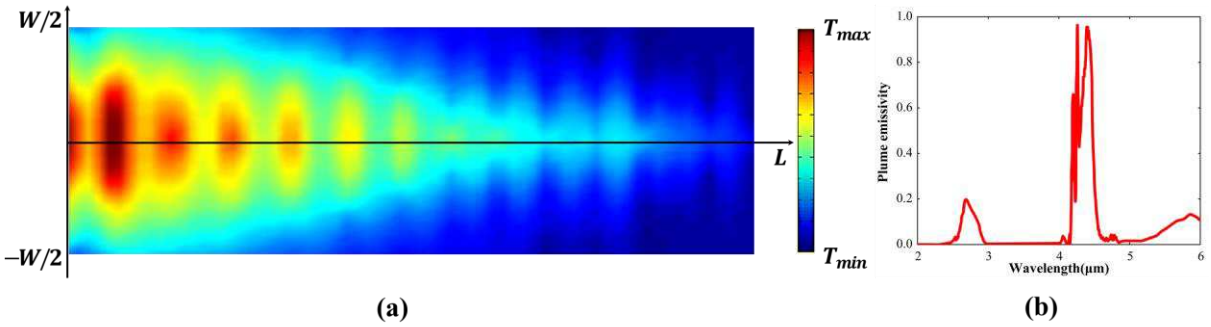

Fig. 1 Radiation signature of the aircraft plume. (a) Temperature distribution (Yuan, H. et al. 2019). (b) Spectral emissivity.

The infrared signal intensity of the aircraft skin is related to the aerodynamic heating effect of the surrounding atmospheric environment. In contrast, the impact of the sun, sky, and Earth radiation on the aircraft infrared signature can be ignored (Mahulikar, S. P. et al. 2009). Additionally, stealth aircraft incorporate specific surface heat dissipation materials to reduce the average skin temperature. In summary, the average temperature of the aircraft skin can be expressed as

$$T_{skin\_ave} = T_{atm} + C \cdot T_{atm}\left[\beta\left(\frac{v-1}{2}\right)Ma^2\right] \tag{2}$$

where T_{atm} is the ambient atmospheric temperature of the aircraft, β is the temperature recovery coefficient, v is the specific heat capacity ratio, Ma is the flight speed of the aircraft (the unit is Mach number), and $C \approx 0.84$ (Li, N. et al. 2015).

The temperature distribution and spectral emissivity curve of the aircraft plume are the main factors used to analyze the plume radiation signature. S. J. P. Retief presented a radiance inversion technique to construct a three-dimensional radiance model of the plume by actual aircraft plume radiance recordings which can obtain the plume temperature distribution at any observation angle (Retief, S. J. P. 2012; Retief, S. J. P. et al. 2014). Figure 1(a) is a temperature distribution diagram of the plume with length L and width W at the observing sight-line perpendicular to the plane of the aircraft (Retief, S. J. P. 2012). The plume is a selective radiator, and its spectral emissivity curve is shown in Figure 1(b) (Rao, G. A. et al. 2013; Yuan, H. et al. 2019; Yuan, H. et al. 2019).

The plume radiant intensity calculation model is shown as follows. The plume temperature distribution diagram is divided into two-dimensional grids, with $P \times Q$ pixels, and the temperature of each grid is T_i. The plume spectral radiant intensity $I_{plume}(\lambda)$ can be calculated through the superposition method and expressed as

$$I_{plume}(\lambda) = \varepsilon_{plume}(\lambda)\sum_{i=1}^{P\times Q}\frac{M(T_i,\lambda)}{\pi}A_{grid} \tag{3}$$

Where $\varepsilon_{plume}(\lambda)$ is the plume spectral infrared emissivity, $M(T_i,\lambda)$ is the spectral radiant emittance of the grid i, A_{grid} is the projected area of each grid and expressed as $A_{grid} = (L \times W)/(P \times Q)$.

2.2 Signal response of an infrared detection system

A space-based remote sensing platform has unique advantages compared with the traditional platforms, such as early detection, wide-area detection, continuous monitoring, high detection

efficiency, and good detection direction. The space-based platform is an effective means to improve the ability to monitor the battlefield. Figure 2 shows a diagram of an aircraft target and Earth background being detected by a space-based infrared system. The detector whose field of view covers the aircraft target is called the target detector (TD). The other detectors (BD), image the Earth background as well as the aircraft target.

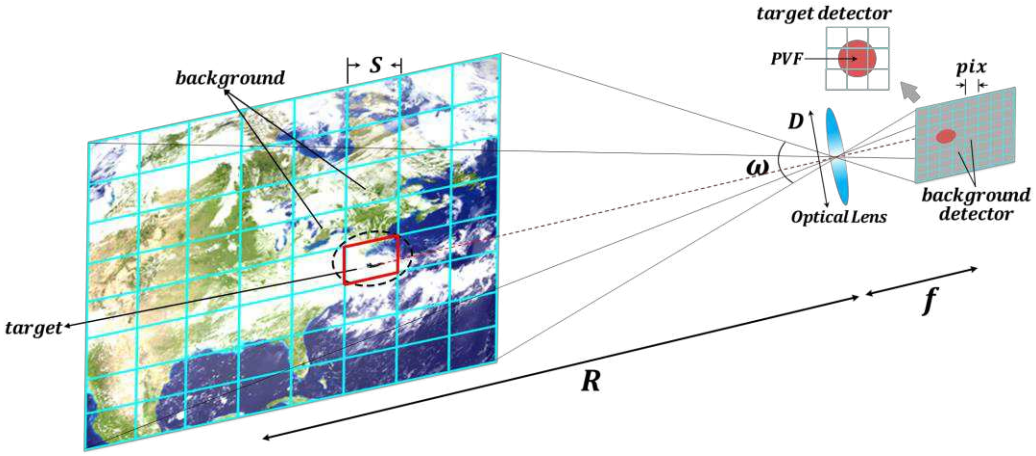

Fig. 2 Aircraft target detection schematic in Earth background.

The aircraft solid angular subtense is much less than the background detector solid angular subtense, as a result of which the aircraft is considered to be a point source. The point source is diffracted by the optical system to form a Fraunhofer diffraction ring and only a fraction of the signal falls on the target detector, as shown in Figure 2. The fraction is the point visibility factor (*PVF*), i.e., encircled energy (Holst, G. C.. 2017; Yang, T. et al. 2017).

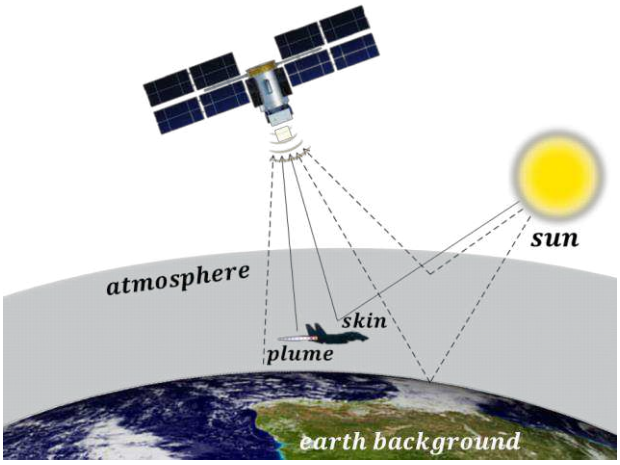

Fig. 3 Radiation information sources.

According to Figure 2, the infrared radiation of the aircraft target and the Earth background are collected by the detector array through the optical system and converted into electrons stored in the integrating capacitor. The response electron numbers (REN) of the TD and BD can be expressed as

$$N_{TD} = \left(L_{q,back} \left(S^2 - A_{aircraft} \right) + I_{q,aircraf} PVF \right) A_{opt} \tau_{opt} \eta T_{\text{int}} / \left(R^2 \right) + T_{\text{int}} I_{dark} / q \tag{4}$$

$$N_{BD} = L_{q,back} S^2 A_{opt} \tau_{opt} \eta T_{\text{int}} / \left(R^2 \right) + T_{\text{int}} I_{dark} / q \tag{5}$$

Where A_{opt} is the entrance pupil area, τ_{opt} is the optical transmittance, and η is the quantum efficiency. I_{dark} is the dark current of the detector system, and q is the quantity of electric charge, where $q = 1.6 \times 10^{-19} C$. $A_{aircraft}$ is the projected area of the aircraft in the system imaging direction, including the skin and plume. S is the system spatial resolution,

expressed as $S = pix \cdot R/f$, as shown in Figure 2. T_{int} is the integration time which is limited by three factors. During the integration time, the system REN cannot be oversaturated, the aircraft target flying distance cannot be longer than S, and the movement distance of the sensor nadir point cannot be longer than S. Therefore, T_{int} needs to satisfy

$$T_{\text{int}} \le \min\left\{N_{full}/P_{TD}, S/v_{aircraft}, S/v_{sub}\right\} \tag{6}$$

$$P_{TD} = \left(L_{q,back}\left(S^2 - A_{aircraft}\right) + I_{q,aircraf}PVF\right)A_{opt}\tau_{opt}\eta/\left(R^2\right) + I_{dark}/q \tag{7}$$

where N_{full} is the detector full well capacity, $v_{aircraft}$ is the aircraft flying velocity, and v_{sub} is the nadir point velocity of the satellite. $I_{q,aircraf}$ is the aircraft radiant intensity at the system entrance pupil, as shown in Figure 3, that includes skin and plume self-radiation through the atmospheric attenuation as well as the atmospheric path radiant intensity I_{path}. Therefore, $I_{q,aircraf}$ can be expressed as

$$I_{q,aircraf} = \int_{\lambda_1}^{\lambda_2} \frac{\lambda}{hc}\left(\tau_{atm}(\lambda)\left(I_{skin}(\lambda) + I_{plume}(\lambda) + I_{path}(\lambda)\right)\right)d\lambda \tag{8}$$

where τ_{atm} is the atmospheric transmittance between the aircraft and the infrared system, λ_1 and λ_2 indicate the spectral response range of the system $L_{q,back}$ is the total background radiance, as shown in Figure 3, which is a superposition of the following four sources: self-radiance of the atmosphere L_{atm}, the scattering radiance of solar by the atmosphere L_{scat}, the self-radiance of the Earth surface through the atmosphere L_{earth}, and the reflected solar radiance by the Earth's surface (albedo) through the atmosphere L_{ref}. Therefore, $L_{q,back}$ can be expressed as

$$L_{q,back} = \int_{\lambda_1}^{\lambda_2} \frac{\lambda}{hc}\left(L_{scat}(\lambda) + L_{ref}(\lambda) + L_{earth}(\lambda) + L_{atm}(\lambda)\right)d\lambda \tag{9}$$

The system performance is limited by noise, which is characterized by the fluctuation of the signal REN and is expressed as

$$noise = \sqrt{N_{TD} + {n_{elec}}^2 + {n_{read}}^2} \tag{10}$$

where n_{read} is the readout noise of the detector, and n_{elec} is information acquisition circuit noise.

2.3 Spectrum optimization flow

Signal-to-noise ratio (SNR) is a main indicator describing the infrared system detection capability and is expressed as

$$SNR = \left(N_{TD} - N_{BD}\right)/noise \tag{11}$$

It is generally considered that the detection requirement can be satisfied when the SNR is greater than 10. That is, the threshold signal-to-noise ratio (TNR) is equal to 10.

A methodology of detection spectrum dynamic optimization is proposed using SNR to enhance the detection performance of the system for aircraft targets.

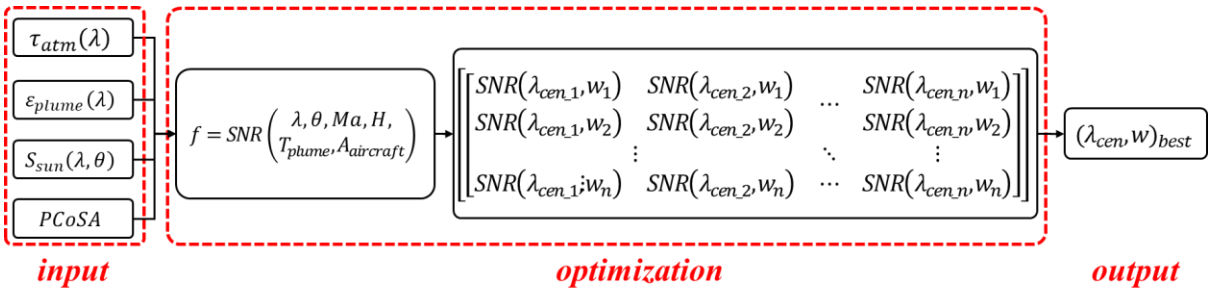

Fig. 4 Flow chart of detection spectrum optimization.

Figure 4 is a flow chart of the detection spectrum dynamic optimization. The optimization steps are as follows:

(1) Initially screen the appropriate broad-spectrum range according to the distribution curve of plume spectral emissivity and atmospheric transmittance. Set 2~5μm here;

(2) Establish a fine mathematical model of SNR based on input spectral parameters, including $\tau_{atm}(\lambda)$, $\varepsilon_{plume}(\lambda)$, $S_{sun}(\lambda,\theta)$, $PCoSA$ (i.e., physical characteristics of the stealth aircraft);

(3) Preset a spectrum width set $\{\omega_m\}$ and central wavelength set $\{\lambda_{cen\_n}\}$. Set ω_m as

$$\{0.02\mu m, 0.04\mu m, 0.06\mu m, \cdots, 1\mu m\}$$

and λ_{cen_n} as

$$\{2.01\mu m, 2.02\mu m, 2.03\mu m, \cdots, 4.99\mu m\}$$

according to the accuracy of the system spectrum adjustment and the robustness of the system performance;

(4) Calculate the SNR of each spectrum band in the dataset $\{\omega_m, \lambda_{cen\_n}\}$ to form the SNR dataset $\{SNR(\omega_m, \lambda_{cen\_n})\}$;

(6) Select the maximum of $\{SNR(\omega_m, \lambda_{cen\_n})\}$, such that the corresponding detection spectrum band then becomes the candidate spectrum band.

(7) Determine whether the SNR_{sys} in the candidate spectrum band is higher than the threshold. If so, the spectrum band is the optimal detection spectrum in the scene. Otherwise, the aircraft target in the circumstance cannot be detected.

The optimal detection spectrum at different aircraft flying modes and Earth backgrounds is obtained according to the proposed optimization method. The different optimal spectra from different scenes and aircraft flying modes are combined to form an optimal spectrum set.

2. Simulation and analysis

The detection performance of the proposed method is characterized by simulating for both marine and cloud backgrounds. The solar zenith angle is set at 30° in the daytime, and the solar radiation is ignored in the nighttime. F22, as a typical fifth-generation fighter aircraft, is selected to be the aircraft target. The infrared emissivity of the F22's skin is set to 0.5 (Baranwal, N. et al. 2015; Li, N. et al. 2015; Cha, J. H. et al. 2014), the speed is Mach 1, and the plume temperature is 1300K. The superiority of the proposed method is illustrated by comparing it with the traditional fixed-spectrum detection system. The detection system parameters are shown in Table 1.

The response spectrum is dynamically adjustable from 2μm to 5μm and covers the two main peaks of the plume spectral emissivity curve. The detectability of the aircraft with different flying altitudes at different seasons and local time is simulated. The performance advantage of the proposed method is demonstrated through the lowest detectable altitude

(LDA) compared with fixed-spectrum detection systems operating at medium-wave (MW, 4.25~4.50μm) and short-wave (SW, 2.65~2.90μm). LDA corresponds to the flying altitude of the aircraft target corresponding to TNR. The variation of SNR at different spectra under a certain condition is analyzed, and several conclusions and suggestions on spectrum optimization are proposed.

Table 1 system parameters.

Parameter	Value
Orbit Altitude	1000km
Dynamic range	2000:1
Full Well	$3\times10^5e^-$
Spatial resolution	260m

3.1 Lowest detectable altitude

The simulation results at different conditions are shown in Figure 5~7, which describe the SNR of the aircraft target with dynamic-spectrum (DS), SW and MW at different flying altitudes respectively. The TNR is shown in the figures, and the conclusions can be drawn intuitively that the lowest detectable altitude is significantly reduced, which means the dynamic-spectrum detection system has better detection performance.

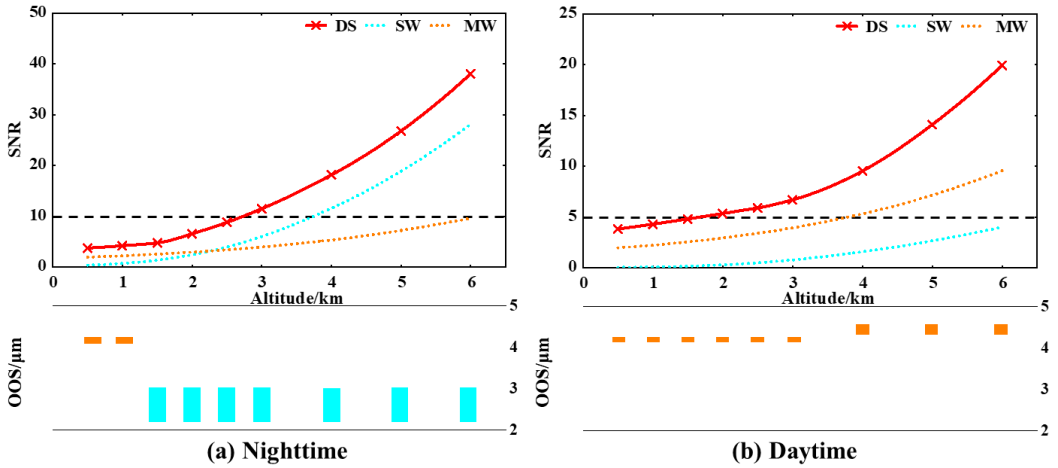

Fig. 5 SNR of the aircraft on marine background in winter.

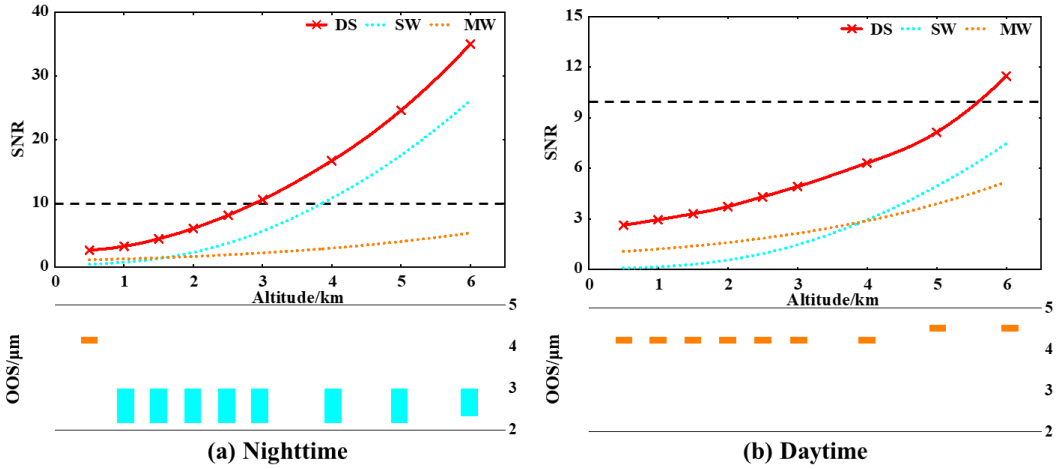

Fig. 6 SNR of the aircraft on marine background in summer

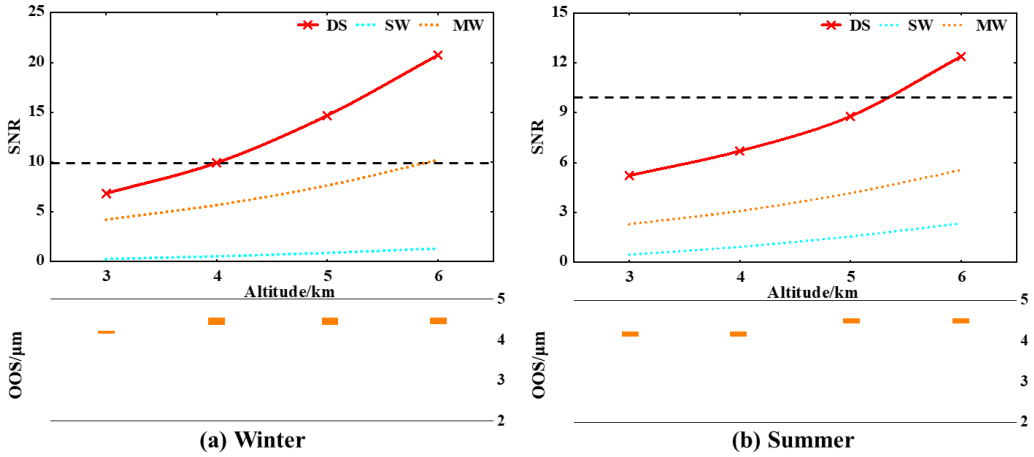

Fig. 7 SNR of the aircraft on cloud background at daytime.

The optimum operating spectra (OOS) at different altitudes of the aircraft target are shown below, and change dynamically under different conditions. The blue bands and orange bands indicate that the optimum spectrum works in the SW range (2~3μm) and MW range (3~5μm). The following conclusions can be obtained:

(1) The central wavelength is mainly focused on 2.63μm, 2.9μm, 4.18μm and 4.45μm, which generate a peak on $f(\lambda)=\varepsilon_{plume}(\lambda)\cdot\tau_{atm}(\lambda)$ at an aircraft flying altitude less than 6km, as shown in Figure 8;

(2) Generally, a narrow spectrum width is beneficial to improve the contrast of the target, but this will reduce the REN and limit the improvement of SNR. The SNR at MW range can be increased by selecting a narrow spectrum width as a result of the high spectral REN. However, the spectral REN at MW range is low, leading to the conclusion that a large spectrum width is needed to increase the luminous flux and improve the SNR.

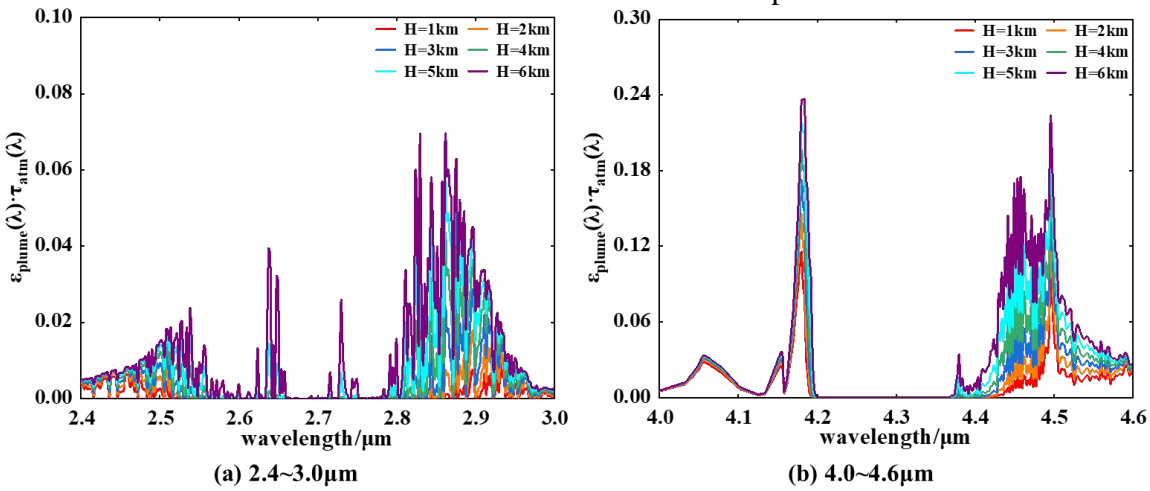

Fig. 8 The value of $f(\lambda)=\varepsilon_{plume}(\lambda)\cdot\tau_{atm}(\lambda)$ at 2.4~3.0μm and 4.0~4.6μm.

3.2 The variation of SNR at different spectrum bands

Taking the simulation conditions of Figure 5(b) and 7(a) as examples, the SNRs of 12,500 spectrum bands were analyzed via the ergodic method. Different spectrum bands were represented by central wavelength and spectrum width. The relationships between SNR and central wavelength, as well as spectrum width, are constructed and shown in Figure 9 and 10 respectively. The following conclusions can be drawn:

(1) The selection of the central wavelength is more important than the spectrum width for the purpose of constructing a detection spectrum with a high SNR which corresponds to the conclusion in Section 3.1.
(2) The choice of spectrum width does not show a clear tendency with the marine background. In contrast, it is more aligned to a narrower spectrum width for the cloud background. This is because the background radiation is too strong in SW range due to solar reflection from the clouds, leading to an optimal detection spectrum in the MW range.

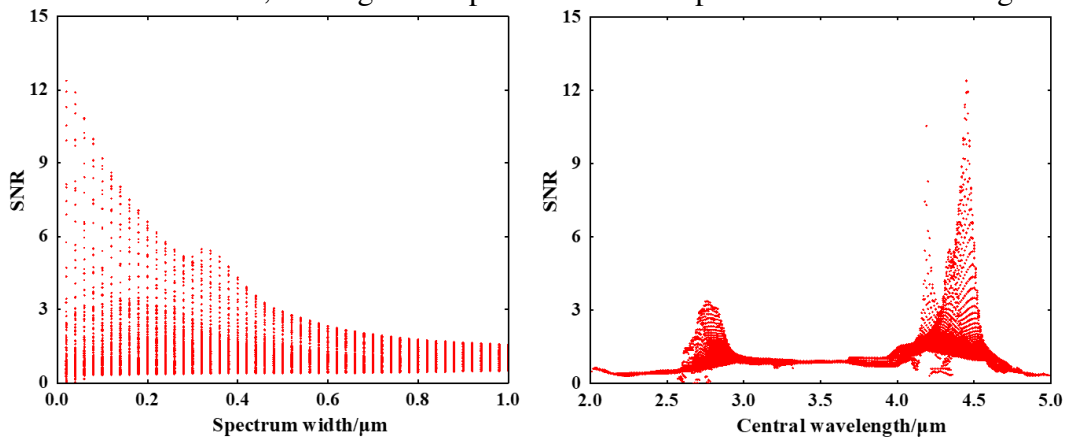

Fig. 9 The variation of SNR with a marine background.

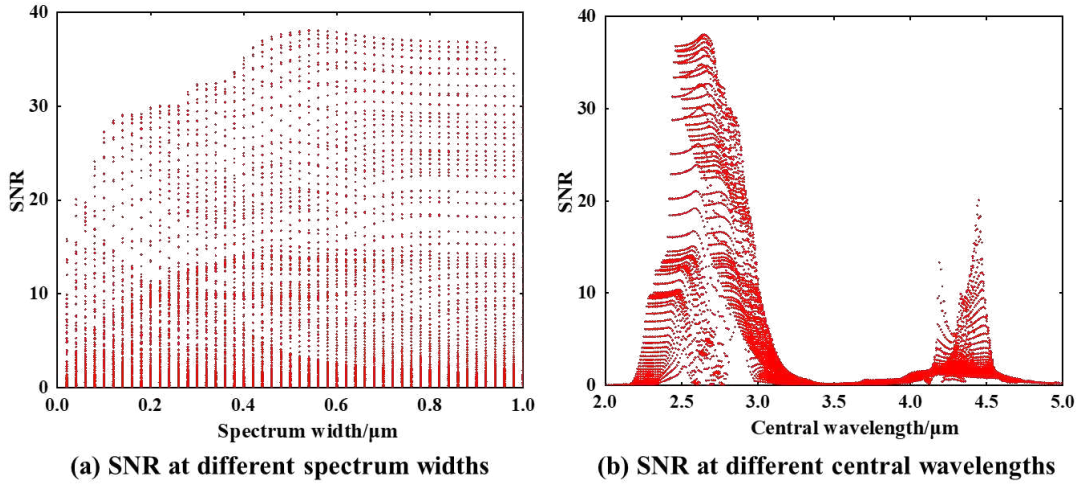

Fig. 10 The variation of SNR with a cloud background.

3. Simulation and analysis

Significant research has been applied to the issue of detecting stealth aircraft targets where there is considerable IR background clutter due to Earth radiation as well as atmospheric attenuation. In this paper, a detection dynamic-spectrum optimization method is proposed based on signal-to-noise ratio. The numerical experiments and simulations show that the dynamic-spectrum system reduces the detectability threshold of aircraft altitudes significantly. The optimal detection spectrum has obvious selectivity for a central wavelength, which can help improve the efficiency of the detection spectrum optimization. The methodology based on detection spectrum dynamic-modulation paves the way to develop efficient and automatic optimization algorithms for detection of high-performance stealth aircraft.

Reference

Baranwal, N., Mahulikar, S. P.: IR Signature Study of Aircraft Engine for Variation in Nozzle

Exit Area. Infrared. Phys. Techn. **74**, 21-27 (2015).
Cha, J. H., Kim, T., Bae, J. Y., Kim, T.: Variation of Supersonic Aircraft Skin Temperature under Different Mach number and Structure. The Korea Institute of Military Science and Technology. **17**(4), 463-470 (2014).
Chen, H., Zhang, H., Xi, Z., Zheng, Q.: Modeling of the turbofan with an ejector nozzle based on infrared prediction. Appl. Therm. Eng. **159**, 113910 (2019).
Cheng, W., Wang, Z., Zhou, L., Shi, J., Sun, X.: Infrared signature of serpentine nozzle with engine swirl. Aerosp. Sci. Technol. **86**, 794-804 (2019);
Gu, B., Wook, B., Jegal, S. H., Choi, S. M., Kim, W. C.: Infrared signature characteristic of a microturbine engine exhaust plume. Infrared. Phys. Techn. **86**, 11-22 (2017).
Holst, G. C.: Point source. In: Electro-Optical Imaging System Performance, 6th Ed. (SPIE 2017).
Hu, Hai., Li, Y., Wei, Z., Zheng, Y.: Optimization of the MSMGWB model used for the calculation of infrared remote sensing signals from hot combustion gases of hydrocarbon fuel. Infrared. Phys. Techn. **107**, 103286 (2020).
Johansson, M., Dalenbring, M.: Calculation of IR signatures from airborne vehicles. Proc. SPIE **6228**, 622813 (2006).
Kou, T., Zhou, Z., Liu, H., Yang, Y., Lu, C.: Multispectral radiation envelope characteristics of aerial infrared targets. Opt. Laser. Technol. **103**, 251-259 (2018).
Kou, T., Zhou, Z., Liu, H., Yang, Y.: Multi-band composite detection and recognition of aerial infrared point targets. Infrared. Phys. Techn. **94**, 102-109 (2018).
Lee, J. H., Chae, J. H., Ha, N. K., Kim, D. G., Jang, H. S.: Efficient Prediction of Aerodynamic Heating of a High Speed Aircraft for IR Signature Analysis. J. Korean Soc. Aeronaut. Space Sci. **47**(11), 769-778 (2019).
Li, N., Lv, Z., Wang, S., Gong, G., Ren, L.: A real-time infrared radiation imaging simulation method of aircraft skin with aerodynamic heating effect. Infrared. Phys. Techn. **71**, 533-541 (2015).
Li, N., Lv, Z., Huai, W., Gong, G.: A simulation method of aircraft plumes for real-time imaging. Infrared. Phys. Techn. **77**, 153-161 (2016).
Mahulikar, S. P., Sane, S., Gaitonde, U., Marathe, A.: Numerical studies of infrared signature levels of complete aircraft. Aeronaut. J. **105**(1046), 185-192 (2001).
Mahulikar, S. P., Rao, G. A., Sane, S. K., Marathe, A. G.: Aircraft plume infrared signature in nonafterburning mode. J. Thermophys. Heat. Tr. **19**(3), 413-415 (2005).
Mahulikar, S. P., Sonawane, H. R., Rao, G. A.: Infrared signature studies of aerospace vehicles. Prog. Aerosp. Sci. **43**(7), 218-245 (2007).
Mahulikar, S. P., Potnuru, S. K., Rao, G. A.: Study of sunshine, skyshine, and Earthshine for aircraft infrared detection. J. Opt. A-Pure. Appl. Op. **11**(4), 45703-45712 (2009).
Nam, J., Chang, I., Lee, Y., Kim, J., Cho, H. H.: Effect of Flight Altitude on Minimal Infrared Signature of Combat Aircraft. Journal of the Computational Structural Engineering Institute of Korea. 375-382 (2020).
Pan, X., Wang, X., Wang, R., Wang, L.: Infrared radiation and stealth characteristics prediction for supersonic aircraft with uncertainty. Infrared. Phys. Techn. **73**, 238-250 (2015).
Rao, G. A., Mahulikar., S. P.: Aircraft Powerplant and Plume Infrared Signature Modelling and Analysis. Aiaa. J. (2013).
Retief, S. J. P.: Aircraft plume infrared radiance inversion and subsequent simulation model. Proc. SPIE **8543**, 85430P (2012).
Retief, S. J. P., Dreyer, M. M., Brink, C.: Infrared recordings for characterizing an aircraft plume. Proc. SPIE **9257**, 92570C (2014).
Sircilli, F., Retief, S. J. P., Magalhaes, L. B., Ribeiro, L. R., Zanandrea, A., Brink, C.,

Nascimento, M., Dreyer, M. M.: Measurements of a micro gas turbine plume and data reduction for the purpose of infrared signature modeling. IEEE. T. Aero. Elec. Sys. **51**(4), 3282-3293 (2015).

Sun, W., Wang, S. B.: Study on Infrared Images Simulation of Fighter Aircraft. International Conference on Control, Automation and Systems (ICCAS), pp. 1703-1708 (2019).

Veiga, IV.: IR Signature Modelling at BAE Systems ATC. International Target and Background Modeling and Simulation Workshop, ONERA, pp. 1–26 (2011).

Wang, Y., Xie, F., Wang, J.: Short-wave infrared signature and detection of aircraft in flight based on space-borne hyperspectral imagery. Chin. Opt. Lett. **14**(12), 132-135 (2016).

Wu, S., Zhang, K., Niu, S., Yan, J.: Anti-Interference Aircraft-Tracking Method in Infrared Imagery. Sensors. **19**, 1289 (2019).

Willers, C. J., Willers, M. S., Waal, A.: Aircraft vulnerability analysis by modeling and simulation. Proc. SPIE **9251**, 92510M (2014).

Yang, T., Zhou, F., Xing, M.: A Method for Calculating the Energy Concentration Degree of Point Target Detection System. Spacecraft Recovery & Remote Sensing. **38**(2), 41-47 (2017).

Yuan, H., Wang, X. R., Guo, B. T., Ren, D., Zhang, W. G., Li, K.: Performance analysis of the infrared imaging system for aircraft plume detection from geostationary orbit. Appl. Opt. **58**(7), 1691–1698 (2019).

Yuan, H., Wang, X., Yuan, Y., Li, K., Zhang, C., Zhao, Z.: Space-based full chain multi-spectral imaging features accurate prediction and analysis for aircraft plume under sea/cloud background. Opt. Express **27**(18), 26027-26043 (2019).

Zhang, T., Xu, Z., Wang, Y., Sun, F., Zhang, H.: Overall optimization design of high temperature components cooling coefficient for lower infrared turbofan engine. Infrared. Phys. Techn. **102**, 102990 (2019).

Zheng, T., Dong, W., Wang, Z.Y., Yi, X.S., Zhao, Y., Yuan, Z.D., Zhao, Y.L.: Investigation of infrared spectral emissivity of low emittance functional coating artefacts. Infrared. Phys. Techn. **110**, 103454 (2020).

Zhou, Y., Wang, Q., Li, T., Hu, H.: A numerical simulation method for aircraft infrared imaging. Infrared. Phys. Techn. **83**, 68-77 (2017).

Zhou, Y., Wang, Q., Li, T.: A new model to simulate infrared radiation from an aircraft exhaust system. Chinese. J. Aeronaut. **30**(2), 651-662 (2017).

Declarations

Dear Editor:

We would like to submit the enclosed manuscript entitled "Detection spectrum optimization of stealth aircraft targets from a space-based infrared platform" by Xinyue Ni(Doc.), Shutian Yu (Doc.), Xiaofeng Su (Prof. And Doc.), Fansheng Chen (Prof. And Doc.), which we wish to be considered for publication in "**OPTICAL AND QUANTUM ELECTRONICS**". I would like to declare on behalf of my co-authors that the work described was original research that has not been published previously. All the authors listed have approved the manuscript that is enclosed.

Detecting stealth aircraft based on a space-based infrared detection system is currently a hot research area. However, the conventional fixed-spectrum detection system cannot satisfy the effective detection to aircraft targets due to complex earth background clutter and atmospheric attenuation. Developing a novel spectrum dynamic-modulation strategy is urgent and indispensable. In our manuscript, we design a detection spectrum optimization method according to the threshold signal-to-noise ratio，and demonstrate the proposed methodology can substantially improve the detection performance of aircraft.

We hope this paper is suitable for "**OPTICAL AND QUANTUM ELECTRONICS**" and we look forward to receiving comments from the reviewers. If you have any queries, please don't hesitate to contact me at the address below.

Funding: National Natural Science Foundation of China (61975222)
Conflicts of interest/Competing interests: Not applicable
Availability of data and material: Not applicable
Code availability: All codes are fully available without restriction
Authors' contributions: Not applicable

Lead author: Xinyue Ni
E-mail: *963330909@qq.com*
Corresponding author: Xiaofeng Su
E-mail: **fishsu@mail.sitp.ac.cn*
Postal address: Key Laboratory of Intelligent Infrared Perception, Shanghai Institute of Technical Physics, Chinese Academy of Sciences, 500 Yu Tian Road, Shanghai, 200083, China

Thank you and best regards.
Yours sincerely,
Prof. Doc. Xiaofeng Su
March 10, 2021

Figures

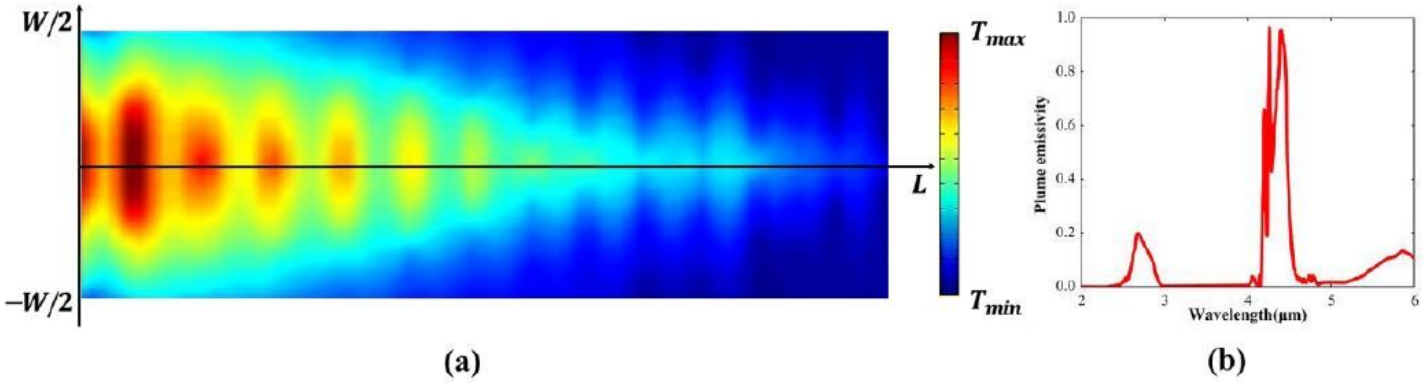

Figure 1

Radiation signature of the aircraft plume. (a) Temperature distribution (Yuan, H. et al. 2019). (b) Spectral emissivity.

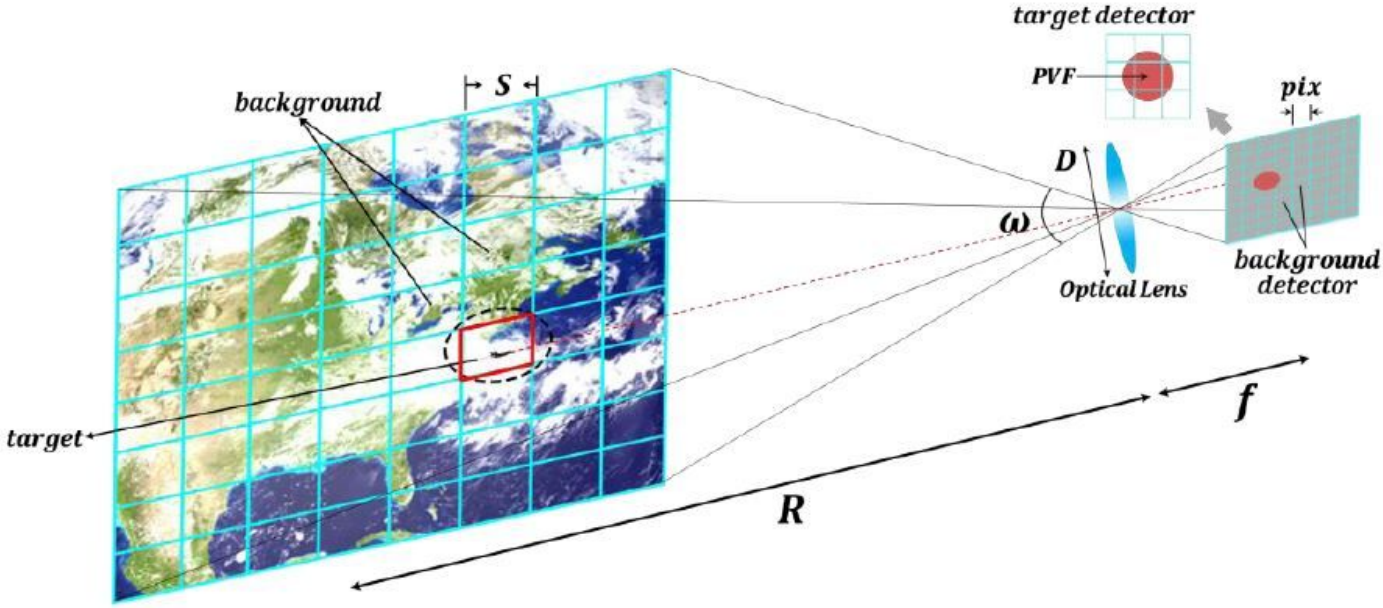

Figure 2

Aircraft target detection schematic in Earth background.

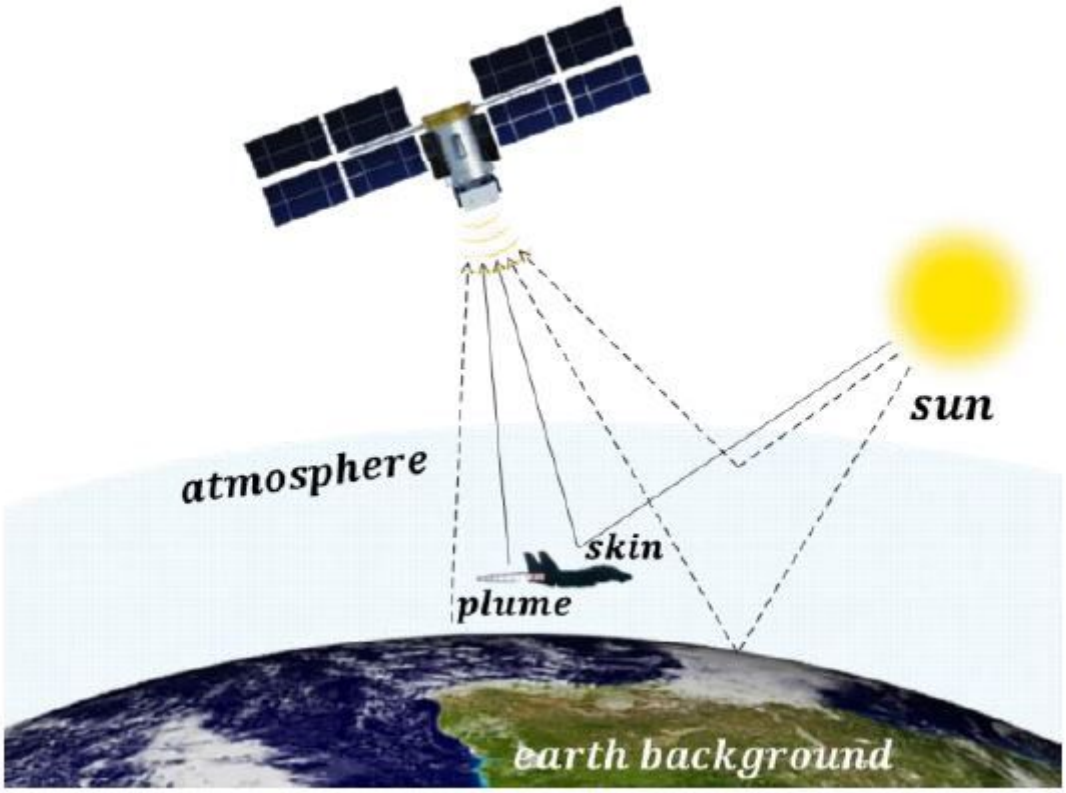

Figure 3

Radiation information sources.

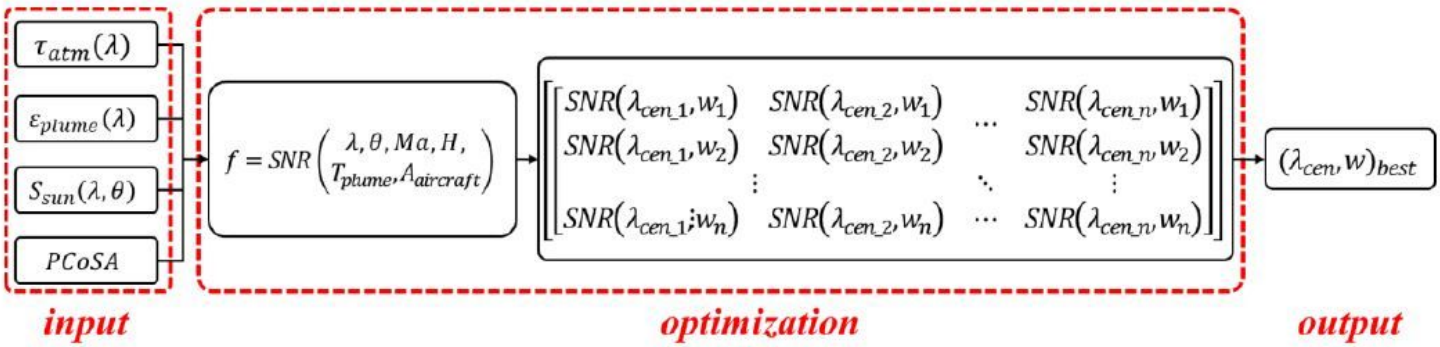

Figure 4

Flow chart of detection spectrum optimization.

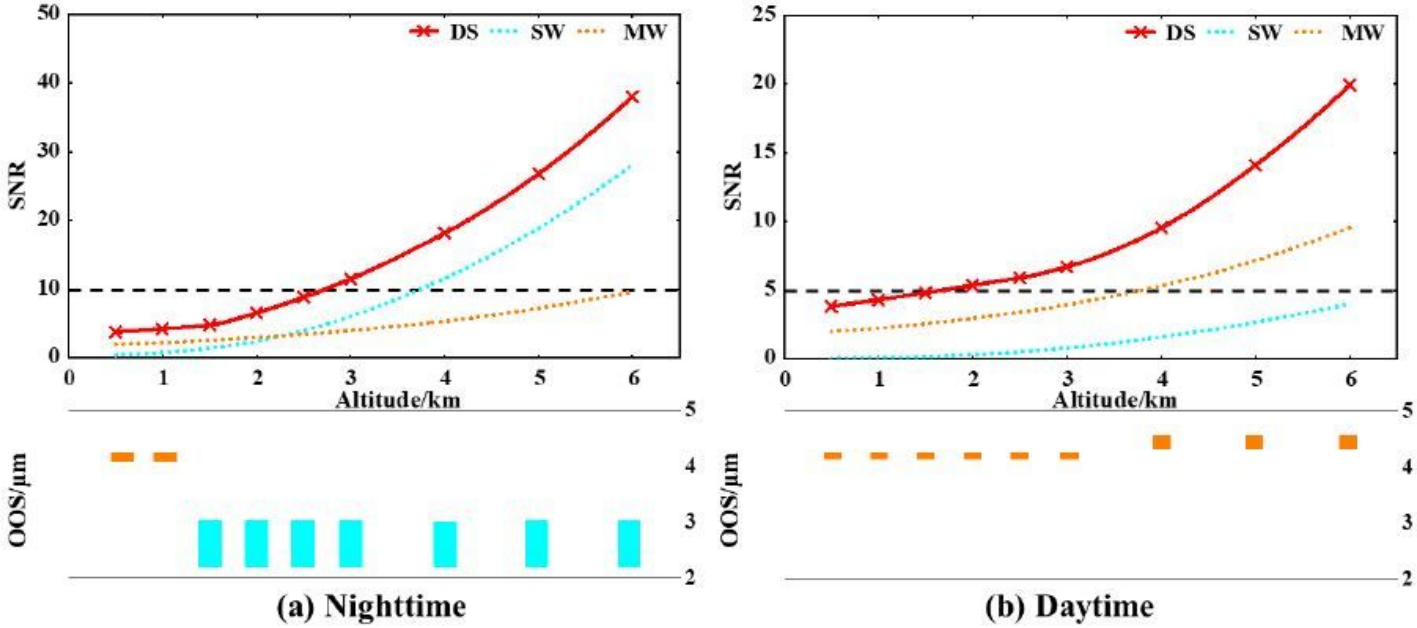

Figure 5

SNR of the aircraft on marine background in winter.

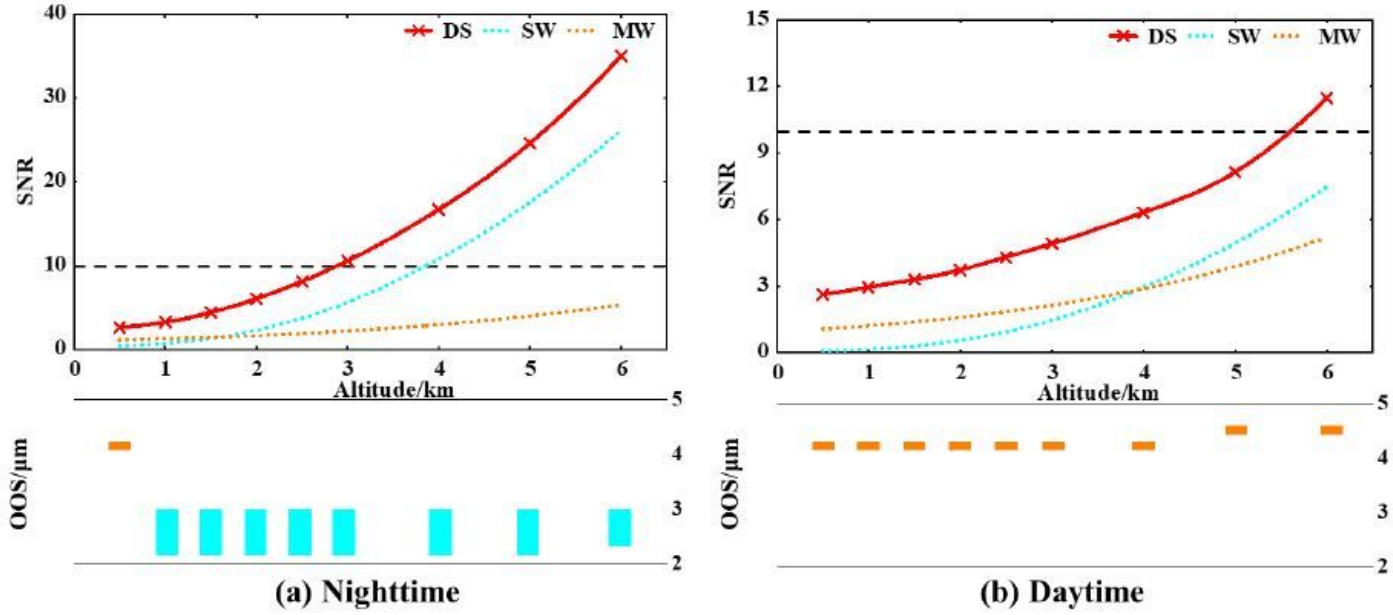

Figure 6

SNR of the aircraft on marine background in summer

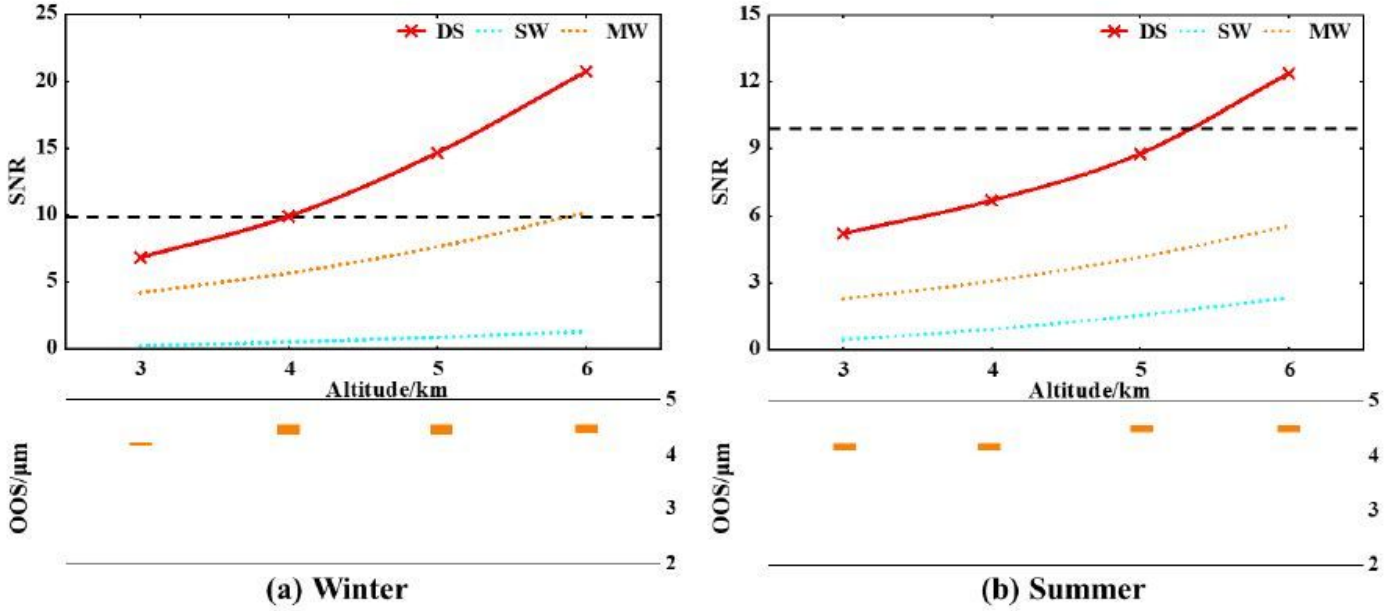

Figure 7

SNR of the aircraft on cloud background at daytime.

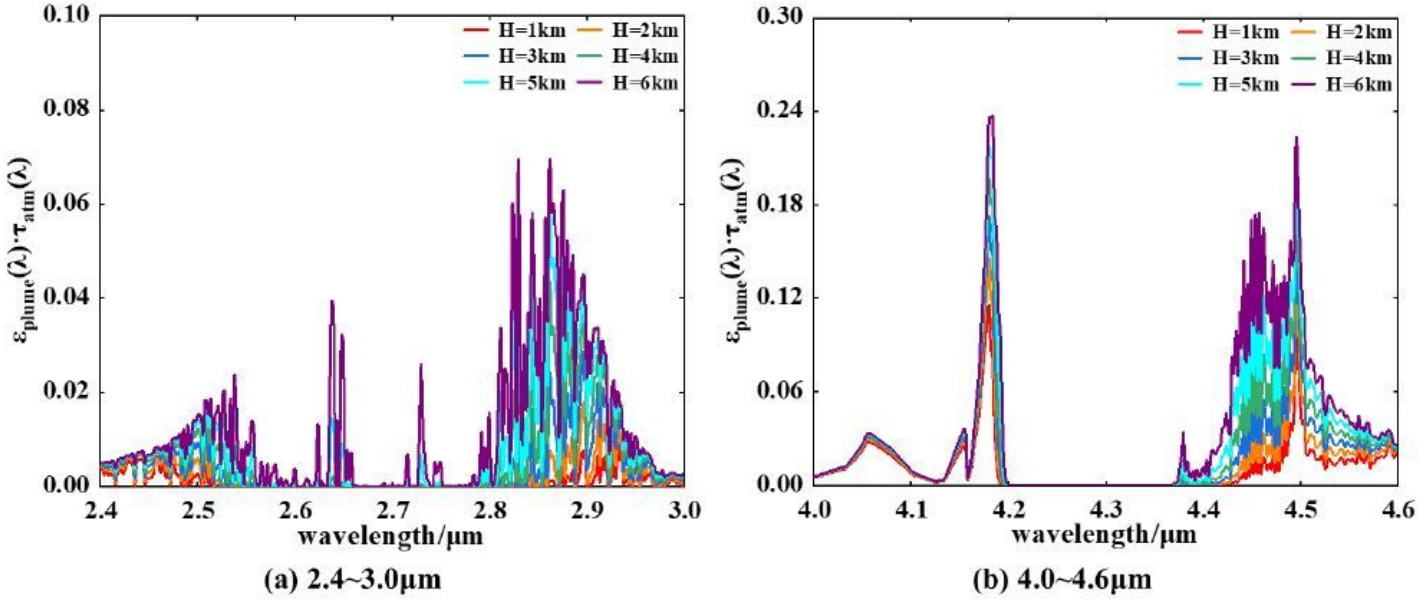

Figure 8

The value of f(λ) = εplume(λ) · τatm(λ) at 2.4~3.0μm and 4.0~4.6μm.

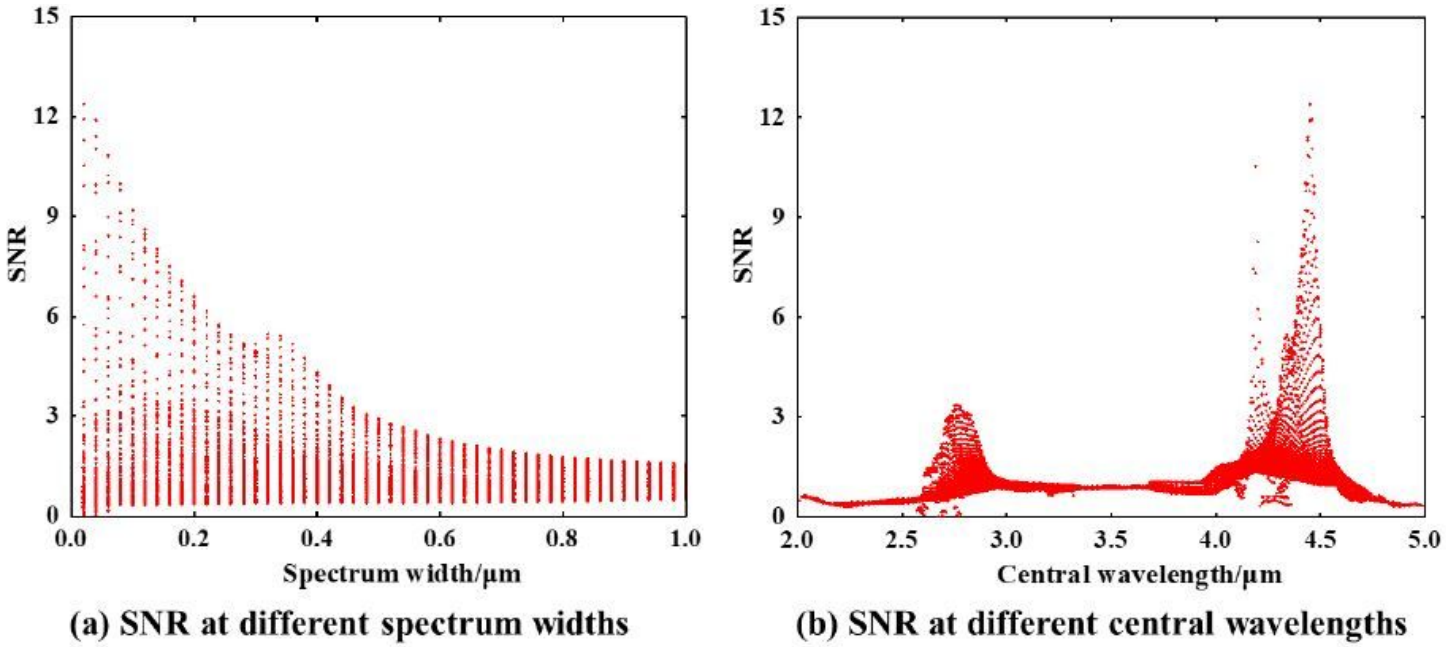

(a) SNR at different spectrum widths (b) SNR at different central wavelengths

Figure 9

The variation of SNR with a marine background.

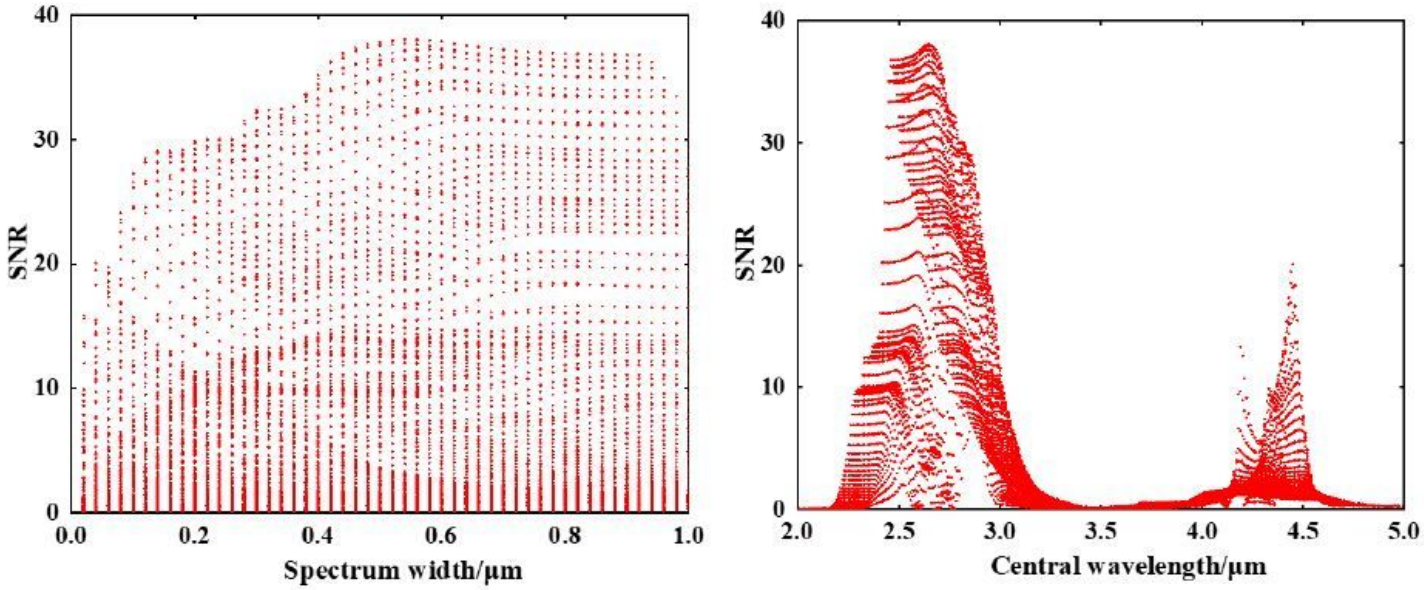

(a) SNR at different spectrum widths (b) SNR at different central wavelengths

Figure 10

The variation of SNR with a cloud background.